

Skeleton-Sectional Structural Analysis for 3D Printing

Wen-Peng Xu^{1,2}, *Member, CCF*, Wei Li¹, and Li-Gang Liu^{1,*}, *Member, CCF*

¹*School of Mathematical Sciences, University of Science and Technology of China, Hefei 230026, China*

²*School of Computer Science and Technology, Henan Polytechnic University, Jiaozuo 454100, China*

E-mail: wpxu08@gmail.com; lw15@mail.ustc.edu.cn; lgliu@ustc.edu.cn

Received December 1, 2015; revised February 26, 2016.

Abstract 3D printing has become popular and has been widely used in various applications in recent years. More and more home users have motivation to design their own models and then fabricate them using 3D printers. However, the printed objects may have some structural or stress defects as the users may be lack of knowledge on stress analysis on 3D models. In this paper, we present an approach to help users analyze a model's structural strength while designing its shape. We adopt sectional structural analysis instead of conventional FEM (Finite Element Method) analysis which is computationally expensive. Based on sectional structural analysis, our approach imports skeletons to assist in integrating mesh designing, strength computing and mesh correction well. Skeletons can also guide sections building and load calculation for analysis. For weak regions with high stress over a threshold value in the model from analysis result, our system corrects them by scaling the corresponding bones of skeleton so as to make these regions stiff enough. A number of experiments have demonstrated the applicability and practicability of our approach.

Keywords 3D printing, sectional structural analysis, skeleton, mesh correction

1 Introduction

With the rapid progress of 3D printing technology, it has been proved to be an important tool for rapid prototyping, also known as additive or layered manufacturing. 3D printing is very convenient to manufacture physical objects from digital models with simple operations and no skill requirements. As its technology matures, 3D printing has become more common and cheaper to use. The creation of a 3D printed object is achieved by additive process, which produces an object by laying down successive layers of materials until the entire object is built up. Each of these layers can be seen as a thin horizontal slice of the eventual object with various types of technologies, such as selective laser sintering (SLS), stereolithography (SLA) and fused deposition modeling (FDM). Increasingly inexpensive 3D printers and various software packages make common people easily realize their own design.

Most of 3D digital models are likely to be improperly manufactured and fragile in daily use, because they are probably designed by users with little manufacturing experience. What is worse, maybe the final output objects of printers differ a lot from what users actually want. For instance, if a user input a model that is poorly designed into a 3D printer, it may end up with a broken object. Therefore most designed models, particularly those for complicated objects, require some tweaking and fixing. Fortunately, people have devised ways to help designed models print out in accordance with their plans. Many computational tools have been developed to fix models so as to make them stiffer, such as structural analysis^[1-3], balance analysis of static and rotational objects^[4-5], and deformation behaviors^[6]. Traditionally, most of structural analysis methods adopt the finite element method (FEM) for the accuracy. However, FEM is time-consuming be-

Regular Paper

Special Section of CVM 2016

This work was supported by the National Natural Science Foundation of China under Grant Nos. 61222206 and 11526212, the 100 Talents Project of the Chinese Academy of Sciences, the Science and Technology Project of Henan Province of China under Grant No. 162102310090, and the Key Scientific Research Projects of the Higher Education Institutions of Henan Province of China under Grant No. 16A520011.

*Corresponding Author

©2016 Springer Science + Business Media, LLC & Science Press, China

cause it involves mesh generation and solving process of large linear systems. Moreover, FEM is separated from shape designing. Thus trial-and-error is the most common approach between FEM and shape designing. A recent work aims to integrate FEM and geometric design during the process of shape editing^[7]. But it needs mesh generation and domain decomposition. The tetrahedral meshes generated may have poor qualities, and domain decomposition may downgrade the usability of system.

Another method to compute the stress of models in 3D printing is sectional structural analysis^[3] which is mostly used in mechanics of materials. Considering its abilities, there are three reasons to use it in 3D printing. First, most of the weak parts of 3D models resemble thin tubes. Therefore, we can assume that these components have beam shapes. Second, since bending forces usually result in larger stress than axial forces in most cases, the printed objects are more likely to break by bending forces even if they may suffer from axial forces at the same time. Third, it works well with good accuracy for 3D printing^[3]. In essence, regardless of sectional structural analysis or FEM, they are both the approximate methods to compute stress.

In this paper, we present a system which provides an efficient structural analysis method and helps users to design shapes without structural defects. With our system, users can interactively edit the shape of models easily. And the system detects possible structural problems of the models and then feedbacks the results back to users quickly. According to the detected results, the system can fix the weak regions of the shape automatically. The editing interface of our system is mainly skeleton-driven and we adopt sectional structural analysis for detecting possible structural problems. Compared with the system based on FEM^[7], our system does not need mesh generation or boundary conditions determination for the use of sectional structural analysis method. And what is more, our system is faster and simpler while preserving good results. Therefore it can be easily used by novice users.

Our work has the following contributions.

- We introduce skeletons to sectional structural analysis. Shape design can be easily driven by skeletons. Simultaneously, skeletons can well guide sectional structural analysis. Therefore shape design and analysis are well integrated by skeletons.
- We present a direct correction method based on skeletons to strengthen the weak regions detected from models, which is more efficient than traditional iterative

correction methods. For each weak region, our method calculates a scaling factor according to its weakness level and then corrects it locally and automatically by scaling the corresponding bone.

2 Related Work

2.1 Geometric Processing for 3D Printing

With the rapid development of 3D printing techniques, many researchers recently have concentrated on the geometric processing problems. To make the object fit for the size of 3D printer, Hao *et al.*^[8] proposed an efficient curvature-based partitioning method that decomposes a large-scale model into several parts which are much easier to fabricate. But the method is suitable for only a limited type of models. Luo *et al.*^[9] proposed a framework that automatically decomposes a large model into smaller and printable parts which can be assembled to the original object later. For the balancing problem of 3D printed models, Prevost *et al.*^[4] proposed an approach to assist users in improving the self-balancing ability of a given model by adjusting the center of mass based on the combination of hollowing and deformation. After investigating the unique geometrical properties of spinning objects, Bacher *et al.*^[5] presented an algorithm to optimize some inertial properties and design spinning objects which can rotate smoothly and stably. It is important to reduce a model's interior volume to save the cost of 3D printing. This idea was introduced by Wang *et al.*^[10] In their work, they adopted skin-frame structure to reduce the material cost while preserving the model stability and similarity. Motivated by existing common structures in nature, honeycomb-cells structure^[11] and skeletal structure^[12] were proposed to reduce the interior material cost of models.

To detect possible structural problems of printed objects, Telea and Jalba^[13] proposed a method to find thin regions and then used a set of geometric rules to assess the printability of the models. To remove structural defects of 3D models, many researchers have paid their attention to the structural analysis of 3D printing. A method that strengthens a model by hollowing, thickening and strut insertion was presented^[1]. Zhou *et al.*^[2] presented a fast method to search the worst load distribution that may break or severely deform the printed object. A sectional structural analysis method was proposed to optimize the orientation of 3D models to increase their mechanical strength^[3]. A shape editing system integrated with

FEM simulation was introduced^[7] to provide users with structural analysis result feedback. In addition, there are many studies related to appearance research, such as subsurface scattering^[14-17], spatially varying reflectance^[18-23], deformation behavior^[6], and multi-material fabrication^[24].

Our work is mostly similar to [7]. In contrast, we use skeleton-sectional structural analysis to compute the stress of models. Considering the usage of a given 3D printed object, we determine its most possible load. Then according to the analysis result, we provide a direct correction algorithm to strengthen the weak regions of the model.

2.2 Joint Mechanism Design

3D printing can not only output very complex models, but also provide an opportunity to fabricate complicated designed models with excellent mechanical properties which are difficult to manufacture in conventional ways. Therefore, more and more mechanical designs have appeared in recent years. Current researches in this field can be divided into two categories: 1) static mechanical designs, such as the interlocking puzzles^[25] and burr puzzles block^[26], which assemble some pieces together to form a stable shape; 2) dynamic mechanism designs such as motion mechanism^[27-29], joint mechanism^[30-31] and non-assembly mechanism^[32-33]. Such mechanical models can be active or in motion.

In 3D printing, it is naturally expected to print a functional and posable model without the need of manual assembly of its components. Skeletons and joints are important tools in character animation. When a mesh is bounded to a skeleton using skinning, it then follows or reacts according to the transformations of the skeleton's joints and bones.

For this reason, skeletons and joints were imported to help create posable models in 3D printing by Bächer *et al.*^[30] and Cali *et al.*^[31] In overall view of their processes, these two methods are generally similar, and can be briefly summarized as follows: given an input mesh with skin, they first analyzed the skinning weights and their link correspondences to segment the original geometry into an approximate set of body parts. Then from this segmentation, they derived a filtered set of oriented joint locations to assemble all parts. In their research, skeletons and joints are applied to segment and link the model, while in our system they are used to guide sectional structural analysis.

2.3 Skeleton Extraction

A skeleton represents a simplified version of the geometry and topology of a 3D object. It is an effective tool for shape analysis and manipulation, such as character animation and morphing. Therefore skeleton extraction is an important problem in computer graphics which has attracted a lot of attention in recent decades. However, a simple and robust method of skeleton extraction remains a challenge^[34].

Current methods for skeleton extraction can be classified into two main categories, depending on whether methods are working on meshes or point clouds. Skeleton extraction methods for meshes depend on mesh connectivity, which include surface contraction via mesh curvature flow^[35-37], coupled graph contraction and surface clustering^[38], medial geodesic function^[39], reeb graph construction^[40], and mesh decomposition^[41].

More and more methods are designed to work on point clouds. Representative approaches include deformable model evolution^[42-43], extended Laplacian-based contraction^[44], tree data^[45], generalized rotational symmetry axis^[46], and also reeb graph construction^[47-48].

The skeleton above is curve-skeleton. Another related structure is bone-skeleton. Such bone-skeletons can be easily obtained from curve-skeletons by down-sampling. In this paper, we use bone-skeletons to achieve our goal, which can be manually constructed based on the input mesh by 3D computer graphics softwares or down-sampled from curve-skeletons.

3 Overview

The goal of our system is to analyze and optimize structural strength of an input 3D model based on skeleton-sectional structural analysis method. Our system directly takes a mesh as its input. Its pipeline is briefly introduced in Fig.1.

Skeleton Construction and Skin Binding. As mentioned above, a bone-skeleton can be obtained from curve-skeleton or constructed manually based on the input mesh by 3D computer graphics software, such as Maya^①. When building the skeleton, we should set its root joint near the barycenter of the model. Each bone direction should reflect the medial axis of the associated region as much as possible, because we will build sections by the bone direction in the subsequent step.

^①Autodesk Inc. Building skeletons. <https://knowledge.autodesk.com/support/maya/learn-explore/caas/CloudHelp/cloudhelp/2015/ENU/Maya/files/CSS-Building-skeletons-htm.html>, Jan. 2016.

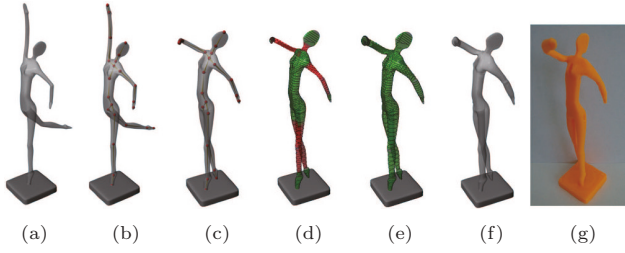


Fig.1. Pipeline of our system. (a) Original mesh. (b) A skeleton is constructed from the original mesh. (c) The mesh is edited by the modification of skeleton. (d) Section structural analysis on the edited mesh tries to detect the possible weak regions. (e) The edited mesh is corrected to strengthen its weak regions by scaling operation. (f) Final mesh after editing and correction. (g) Photo of model printed from the corrected mesh.

To provide a convenient deformation driven by the skeleton, we can use skin binding method in Maya directly or Pinocchio system^[49] to rig the input mesh to the skeleton. After skin binding, the association is built between the input mesh and the skeleton. And the skeleton can be used as the editing medium of the input mesh.

Shape Editing. After skin binding, the input mesh can be edited by controlling the skeleton. That is to say, all the regions of the mesh can be translated, rotated and scaled by adjusting the associated bones according to a user's design.

Sectional Structural Analysis. After editing the mesh, we use sectional structural analysis on the designed mesh to detect possible structural problems. Our system considers the worst-case load for every section of the model and computes the stress distribution of the model. From the analysis result, we can more easily edit the mesh in order to ensure the final model away from structural defects.

Local Scaling Correction. Considering the materials used in 3D printing, we assume that models will break if their stress is larger than a stress threshold. From the previous analysis steps, the region whose stress is larger than the stress threshold is found out and then corrected by reducing its stress to a permissible range.

4 Sectional Structural Analysis

4.1 Preliminaries

We use an anisotropic linear material model and linear elasticity equations to model the object behavior for the purpose of stress analysis. That is, stress is proportional to the strain with a constant factor E as:

$$\sigma = E\varepsilon, \quad (1)$$

where σ and ε are the stress and the strain of a point in the structure respectively, and E is elastic modulus of the material.

For most of the weak components, shapes are similar to thin tubes in 3D printing. It is reasonable to assume that the weak components have beam shapes with sections. We take Euler-Bernoulli assumption as the basis of sectional structural analysis^[3]. This assumption is widely adopted in the field of engineering. The accuracy increases with the lengthening of section thins and moment-arms. From this assumption, the strain can be expressed as

$$\varepsilon = \frac{B'B}{AB} = \frac{y d\theta}{AB} = \frac{y}{\rho}, \quad (2)$$

where AB is the original length of the observed unit, $B'B$ is the incremental length of AB , y is the distance from point A to the neutral axis O_1O_2 , θ is the angle between the two sections, and ρ is the curvature radius of the neutral axis near the current sections^[50], as shown in Fig.2.

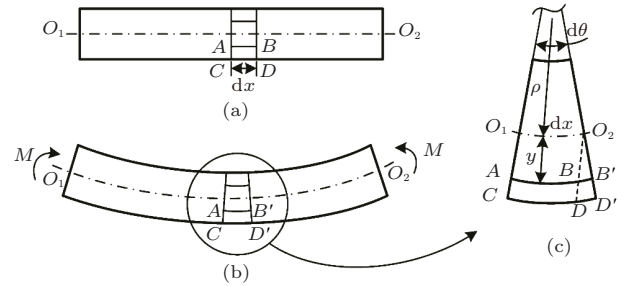


Fig.2. Deformation of a beam. (a) Rest shape. (b) Deformed shape. (c) Detail view of the deformation in a local part.

For a 3D printing object, the imposed load is probably moments and axial forces in most cases. In general, moment will result in larger stress than axial forces. Thus we can regard the moment as the main imposed load for simplicity. Based on this assumption and the moment equilibrium, we can get the equation as

$$\int_A \sigma_x y dA = M, \quad (3)$$

where σ_x is the normal stress in x direction, A is the element of the area in the section and M is the moment, as shown in Fig.3.

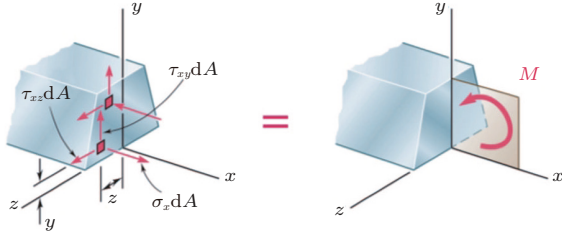


Fig.3. Moment equilibrium.

From (1) and (2), we have

$$\sigma_x = E \frac{y}{\rho}. \quad (4)$$

Substituting for σ_x in (3) by (4), we obtain

$$M = \int_A \sigma_x y dA = \frac{E}{\rho} \int_A y^2 dA = \frac{EI_z}{\rho}, \quad (5)$$

where I_z is the second moment of the area:

$$I_z = \int_A y^2 dA. \quad (6)$$

From (4) and (5), we can obtain the normal stress σ_x at any distance y from the neutral axis:

$$\sigma_x = \frac{My}{I_z}. \quad (7)$$

4.2 Section Modulus

The maximum stress of a section will decide whether the section will fracture or not. Given a specific moment M_z in z direction, from (7), we can obtain the maximum stress as

$$\sigma_{\max} = \frac{M_z y_{\max}}{I_z} = \frac{M_z}{W_z}, \quad (8)$$

with the maximum distance y_{\max} from the neutral axis. W_z is called the section modulus of z direction in the engineering literature:

$$W_z = \frac{I_z}{y_{\max}}.$$

For a 3D printed object, the moment may be imposed with every possible direction. Therefore, the section modulus will vary in different directions. However, there is a minimal value of the section modulus in all directions. We take it as the section modulus for the subsequent stress computing.

It should be noted that flat thin parts can be handled by this method too. For flat thin parts, although

y_{\max} in the thin direction is smaller than the value in the flat direction, the second moment of area in the thin direction is smaller than the value in the flat direction. Then the section modulus in the thin direction will be smaller than the value in the flat direction. Hence, the minimal value of the section modulus mostly is in the thin direction. That is, the maximal stress will appear in the thin direction. This matches the fact that flat thin parts are very weak in the thin direction while they are strong in the flat direction.

4.3 Section Building

Our section building is based on the skeleton of the model. We can simply adopt the direction of the bones as the normal of sections in most cases. Therefore we can build sections at interval h along each bone of the model (we set $h = 8$), as shown in Fig.4. If there are multiple sections in a single slice, we only select the section whose center passes through the bone.

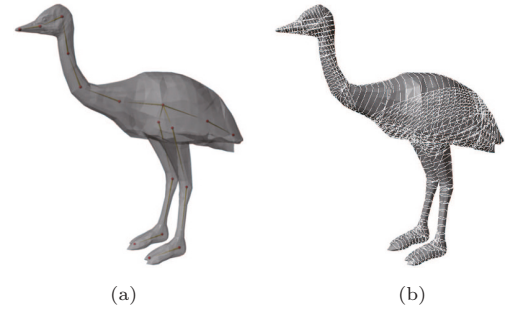


Fig.4. Ostrich model. (a) Input mesh with its skeleton. (b) The mesh and its sections built from the skeleton.

There needs some special process when building sections at the joints which may have more than one direction since they may link several bones. It can be divided into three cases to handle. In the first case, if the joint is the end of the bone, we can take the bone's direction as the normal of the section. In the second case, if the joint is between two bones, we can adopt the average value of the two bone's directions as its normal. In the last case, when the joint is adjacent to more than two bones, we can build several sections whose normals are obtained from the average direction of every two bones.

4.4 Analysis of Loads

It is difficult to consider all the possible loads that a given printed object may be undertaken. But we can analyze the most possible worst-case load for each section of the printed object.

For the physical size of the printed object, we are generally accustomed to holding the main part of the object when an external force is applied on a branch or a cusp of the object (Fig.5(a)). With the skeletons of the object, these constraints are equivalent to the condition when the root joint is fixed and the force is imposed on the branch. Under this configuration, the worst-case load for each branch is applying on the farthest position from the root joint of the object (Fig.5(b)). Because the moment of the root joint becomes larger as the distance lengthens with the same force, the worst-case load for each section in a branch can be defined in a similar way. That means for each section we can find the farthest position to the section from the root joint (Fig.5(c)). If there is more than one farthest point in different branches to a section, we compare all the distances and adopt the farthest position too (Fig.5(d)).

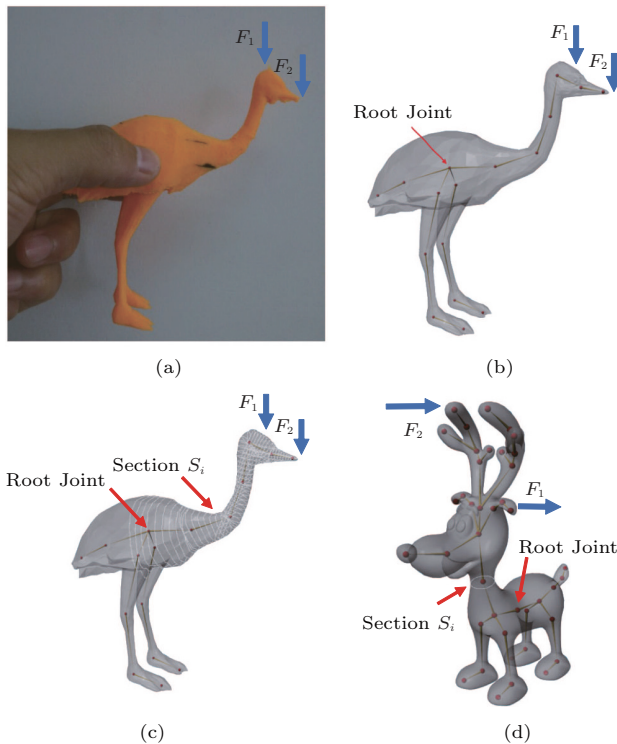


Fig.5. Analysis of loads. (a) The printed object is held by the main part while a force is imposed on a branch. (b) Worst-case load for a branch. (c) Worst-case load for a section. (d) Section with several farthest points in the dog model.

For each section, we can find the farthest distance from the root joint and according to this distance we can compute the maximal moment of each section. Therefore, we can obtain a global maximal moment M_{gmax} for all sections from these moments as the following step.

4.5 Section Safety and Safe Section Modulus

For the printed material, it must have a specific strength threshold $[\sigma]$. If the maximal stress σ_{max} of a section is larger than $[\sigma]$, we regard the section as weak component. Otherwise the section is safe.

From (8), we can obtain the safe section meeting the following requirement:

$$\sigma_{max} = \frac{M_z}{W_z} < [\sigma]. \quad (9)$$

That is:

$$W_z > \frac{M_z}{[\sigma]}, \quad (10)$$

which means the section is safe if its section modulus is satisfied with (10). For a given model, we can obtain a global maximal moment M_{gmax} from the above equations. Then we can acquire a key section modulus W_k as

$$W_k = \frac{M_{gmax}}{[\sigma]}. \quad (11)$$

For each section, if its section modulus W_z is larger than W_k , it is obviously safe because its maximal stress is definitely smaller than $[\sigma]$ in (9). Therefore, the stress of a section whose section modulus is larger than W_k does not need to compute, and this will help to avoid some unnecessary calculation. According to this analysis, we can define W_k as safe section modulus for a given model.

W_k is proportional to M_{gmax} , which depends on the given model and the external force. That is, the bigger force the model is suffered from, the larger W_k is got. For the ostrich model, there are some sections in its back region whose section modulus is larger than its safe section modulus. We display these regions in gray color in Figs.6(b) and 6(c) where the forces are both 20 N. When the force becomes 35 N, its safe section modulus becomes larger too. Therefore there are no sections whose section moduli is larger than the new safe section moduli, as shown in Fig.6(a).

4.6 Algorithm

Based on the analysis above, we can summarize stress computing algorithm as follows.

- 1) According to the result of load analysis, a global maximal moment M_{gmax} can be obtained. Then from (11), we can compute safe section modulus W_k .
- 2) Guided by the skeleton of the model, all sections can be built at interval h along each bone of the skeleton.
- 3) For each section denoted as S_i , perform the following steps:

a) Compute its section modulus W_i . If W_i is larger than W_k , cull section S_i because it is safe enough according to the analysis above, and then go back to step 3; otherwise, go to the next step.

b) Find the farthest distance d from the current section S_i to the end of the branch along the skeleton. Then obtain the maximal moment M_i as

$$M_i = F \times d,$$

where F is an external force imposed on the end of the branch.

c) Calculate the maximal stress σ_{\max} of section S_i from (8).

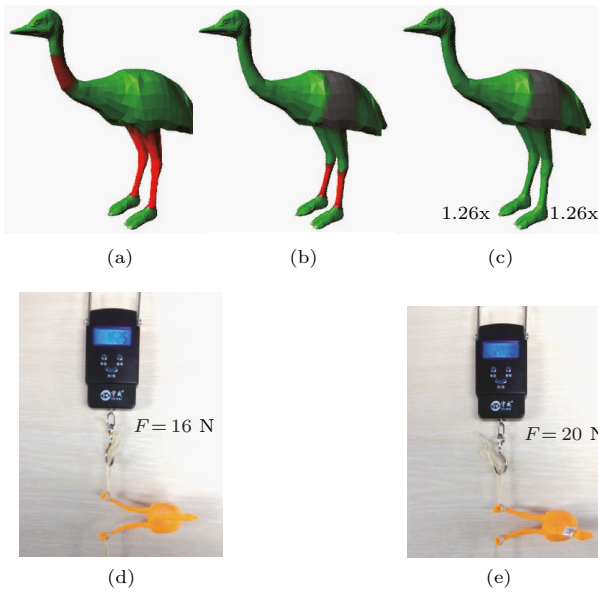


Fig.6. Ostrich experiment. (a) Stress distribution of the original ostrich mesh under a 35 N force. (b) Stress distribution of the original ostrich mesh under a 20 N force. (c) Stress distribution of the corrected ostrich mesh under a 20 N force. (d) The ostrich printed from the original mesh undertakes a 16 N force at most. (e) The ostrich printed from the corrected mesh survives at a force of 20 N.

According to the analysis result, if $\sigma_{\max} > [\sigma]$, the section is weak and fragile. Our system can automatically strengthen the section by the following correction method.

5 Local Scaling Correction

In our system, we assess whether a mesh is safe or not by detecting possible weak sections. That is, if the mesh has no weak section, we think it is safe enough under a given constraint. Therefore, the goal of scaling correction is to change all detected weak sections to safe sections by scaling operation. But we cannot directly scale these sections for this operation may cause

the weak sections to appear in somewhere else. At the same time, this operation may not preserve the shape well with low efficiency.

The sections are related to the domains. Each domain includes several sections. There may be more than one weak section in one domain. Scaling a domain can scale all the sections associated with it. Based on this, we adopt domains as the scaling parts in our system. Compared with scaling sections, scaling domains has a good efficiency and meanwhile it preserves the shape of model well.

We select a domain containing the weakest section to scale in each iteration of scaling correction until there is no domain including weak sections. Firstly we search for the weakest section in the mesh. Secondly we can find the domain related to this section. Finally this domain is scaled with a scaling factor s to eliminate the weakest section.

5.1 Scaling Factor Determining

We scale a domain in order to correct the weakest section to become a safe section. According to this goal, we must determine a domain scaling factor. From the second moment formula (6), it can be obtained that the second moment I of a section is related to t^4 where t is the thickness of the section. Then from (7), it can be deduced that the stress σ caused by moment is related to the section thickness t as

$$\sigma = \frac{C_b}{t^3}, \quad (12)$$

where C_b is a constant value for a given specific position on the mesh which is independent of the section thickness t .

From (12), we compute thickness t_d when σ reaches threshold $[\sigma]$ as

$$t_d = \sqrt[3]{\frac{C_b}{[\sigma]}},$$

where t_d is the target thickness. And now this section is safe enough and not so easy to damage.

Then the scaling factor s can be determined as

$$s = \frac{t_d}{t_m} = \frac{\sqrt[3]{\frac{C_b}{[\sigma]}}}{\sqrt[3]{\frac{C_b}{\sigma_{\max}}}} = \sqrt[3]{\frac{\sigma_{\max}}{[\sigma]}},$$

where σ_{\max} and t_m are the current section maximal stress and thickness before scaling operation respectively.

5.2 Scaling Correction Algorithm

To conveniently describe the algorithm, we denote the set of weak sections by S_w . During the correction process, the system dynamically maintains this section set S_w . In each iteration, if a section in S_w is corrected from weakness to safety, it will be removed from S_w . In the end, S_w should be empty to assure that there is no weak section in the mesh.

The main steps of our correction algorithm are listed as follows.

1) Initialize the section set S_w by putting all weak sections into S_w .

2) If set S_w is not empty, execute the following steps; otherwise the algorithm ends.

a) Sort set S_w by the section stress in descending order and pop up the weakest section S_0 which has the maximal stress σ_m .

b) Search for domain D_0 which includes the weakest section S_0 .

c) Calculate the scaling factor s_0 as

$$s_0 = \sqrt[3]{\frac{\sigma_{\max}}{[\sigma]}}$$

and scale the domain with this scaling factor.

d) Compute the stress in the mesh and update the weak section set S_w according to the stress result.

In the last step d), we can accelerate computation by culling domains which contain no weak sections because these domains do not need to compute stress again. This acceleration can be accomplished by building a domain set which includes no weak sections to avoid unnecessary stress computations.

6 Experimental Results

We have implemented our system as a plug-in in Maya, which can take advantage of the powerful function of Maya. We selected Maya C++ API (Application Programmer Interface) to develop our plug-in system for it provides better performance than Maya Embedded Language (MEL) and Maya Python API. A number of 3D models were tested in our system on a PC with an Intel i5-3210M 2.5 GHz CPU and 8 GB RAM under Windows OS. Then we fabricated these models by FDM (Fused Deposition Modeling) printer using the Polylactic Acid (PLA) material. The FDM printer we used is the MakerBot Replicator 2 with tray size 285 mm × 153 mm × 155 mm. All the test models were printed with a height of 120 mm except for the

bow model whose length is 150 mm. The parameters of the typical PLA material in our experiments were set with a yielding strength of 60 MPa and Young's modulus of 2300 MPa.

Fig.7 shows an experiment on a bow model. The bow model was simulated when it was pulled by force F ($F = 4$ N) (Fig.7(c)). From the analysis result of our system, it is revealed that the regions near both the ends of the bow model are the weak regions when it is pulled, because the stress of these regions exceeds the yielding strength of the material. Using the algorithm of our system, we scale the weak regions of the model according to the stress distribution in Fig.7(d). After the correction, the weak regions of the bow model have become safe in the same test. Two real bow objects of the original mesh and the corrected mesh are printed respectively. They are tested by pulling with an external force. For the bow printed from the original mesh, it was severely deformed at a 3.6 N force and lost its function. Meanwhile, its large deformation regions matched the high-stress regions in the analysis result in Fig.7(e). The bow printed from the corrected mesh works well with a 4 N force in Fig.7(f).

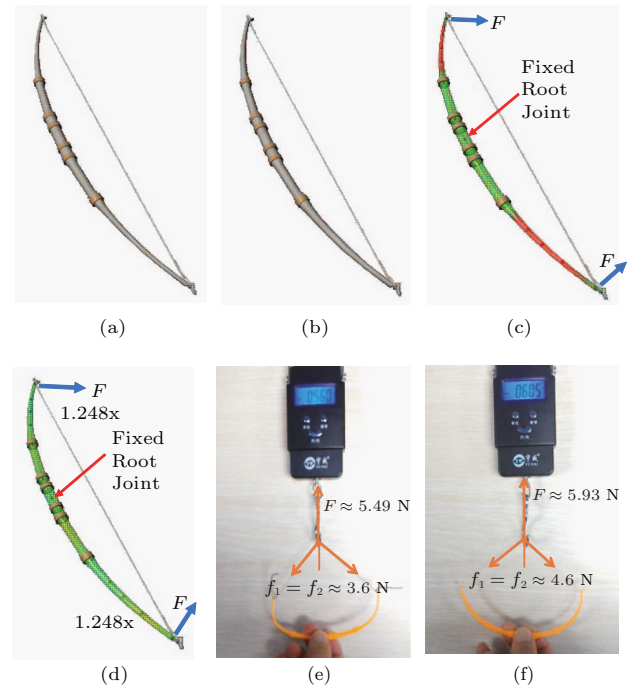


Fig.7. Bow experiment. (a) Original bow mesh. (b) Corrected bow mesh. (c) There are some weak regions on the original bow mesh according to the result of sectional structural analysis. (d) The corrected bow mesh is safe after local scaling correction. (e) The bow printed from the original mesh was severely deformed at a 3.6 N force. (f) The bow printed from the corrected mesh was still fine at a 4.6 N force.

Another experiment on an ostrich model is shown in Fig.6. We fix one leg of the ostrich model and impose a force on the other leg. Considering the symmetry of the model, this constraint is equivalent to that one leg of the model is imposed with a force while the root joint (coincided with the model barycenter) of the ostrich model is fixed. When a force of 20 N is imposed on this ostrich model, it is shown that the leg regions are weak for the reason that their stress is higher than the stress threshold. Then the leg regions of the original mesh are corrected to the safety with our system. The same experiment is conducted on the object printed from the original and the corrected mesh respectively. The experimental result shows that the object printed from the original mesh broke during the experiment while the object printed from the corrected mesh can resist a force of 20 N. Therefore it validates the analysis result of our system. Other two similar examples are shown in Fig.8.

Table 1 lists the statistics of the test models we used. From the table, we can see that the performance of our system depends on the model size and the number of joints. For all test models, our system can finish stress computing and mesh correction within few seconds.

To compare our system with the method of [7], we tested the same dinosaur model, as shown in Figs.8(a) and 8(b) and Table 1. Note that our computational time does not contain the skeleton extraction time, which is in line with [7]. From the results, we can summarize our advantages as follows.

- Our system is faster and more efficient. The time of analysis and optimization in [7] is about 4.6 s and 18.89 s respectively, excluding the time of mesh generation and boundary conditions setting, while our system just spends less than 10 s to finish the same work.

- Our method is simpler and easier. The input of the system of [7] is a tetrahedral mesh which is obtained from mesh generation. It needs to classify the tetrahedron domain into two types, which depends on one or more bones that the domain is associated with. It can

only scale the domains associated with one bone to reduce their stresses. Then it needs to set the boundary conditions to run FEM simulations. We took a mesh as the input of our system directly. Therefore, our system avoids all the studies above so as to make it much easier to use.

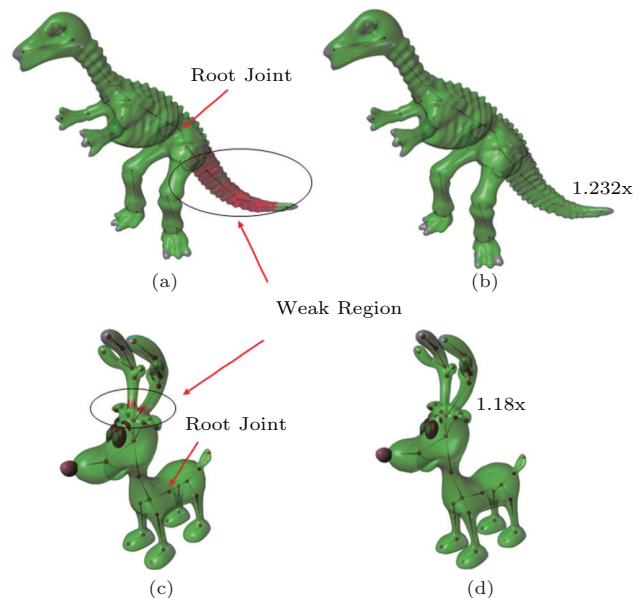


Fig.8. Dinosaur and dog experiments. (a) The tail of the original dinosaur model is weak region. (c) The root of buckhorn in the dog model is weak region. (b) (d) After correction operation the weak regions become safe, and the scaling factors are marked on the figure.

- Since our system is implemented as a plug-in tool in Maya, it has good portability. What is more, it can collaborate with Maya well and thus provide users with more convenience.

7 Conclusions

In this work, we proposed an automatic and practical system to edit and correct a given 3D model for the purpose of improving its structural strength. Skeletons are imported into our system to help to edit the shape

Table 1. Performance of Our System

Model	Joint	Vertex	Face	Section Building (s)	Stress Computing (s)	σ_{\max} (MPa)	Correction (s)
Bow	12	770	1 536	0.27	0.16	77.4	0.31
Ostrich	16	1 643	3 282	1.01	0.66	86.5	0.63
Statuette	22	5 465	10 912	2.65	1.99	175.4	4.28
Dinosaur	23	8 667	17 330	6.51	6.01	110.8	2.88
Dog	40	5 392	10 648	5.42	3.29	67.0	2.28

Note: σ_{\max} is the maximal stress of the model before correction.

and guide sectional structure analysis. A local scaling correction method was provided to strengthen the weak regions while preserving mesh shape well. A number of experimental results have shown the applicability and practicability of our system.

There are several remaining challenges. Our stress computation is an approximation of the actual stress because of skeleton-sectional structure analysis. The other reason is that we only consider the most possible boundary condition which the models may encounter. The system can be improved by enabling users to set arbitrary boundary conditions as a future work. Furthermore, since section building is guided by the skeletons, different skeletons will produce different sections which can affect the analysis result. Another possible future work is to import virtual sections introduced in [3] to solve this problem.

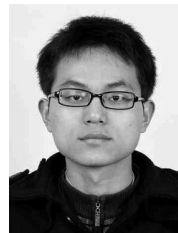
References

- [1] Stava O, Vanek J, Benes B, Carr N, Měch R. Stress relief: Improving structural strength of 3D printable objects. *ACM Transactions on Graphics*, 2012, 31(4): 48:1-48:11.
- [2] Zhou Q, Panetta J, Zorin D. Worst-case structural analysis. *ACM Transactions on Graphics*, 2013, 32(4): 137:1-137:12.
- [3] Umetani N, Schmidt R. Cross-sectional structural analysis for 3D printing optimization. In *Proc. SIGGRAPH Asia Technical Briefs*, November 2013, pp.5:1-5:4.
- [4] Prévost R, Whiting E, Lefebvre S, Sorkine-Hornung O. Make it stand: Balancing shapes for 3D fabrication. *ACM Transactions on Graphics*, 2013, 32(4): 81:1-81:10.
- [5] Bächer M, Whiting E, Bickel B, Sorkine-Hornung O. Spin-it: Optimizing moment of inertia for spinnable objects. *ACM Transactions on Graphics*, 2014, 33(4): 96:1-96:10.
- [6] Bickel B, Bächer M, Otaduy M A, Lee H R, Pfister H, Gross M, Matusik W. Design and fabrication of materials with desired deformation behavior. *ACM Transactions on Graphics*, 2010, 29(4): 63:1-63:10.
- [7] Xie Y, Xu W, Yang Y, Guo X, Zhou K. Agile structural analysis for fabrication-aware shape editing. *Computer Aided Geometric Design*, 2015, 35/36: 163-179.
- [8] Hao J, Fang L, Williams R E. An efficient curvature-based partitioning of large-scale STL models. *Rapid Prototyping Journal*, 2011, 17(2): 116-127.
- [9] Luo L, Baran I, Rusinkiewicz S, Matusik W. Chopper: Partitioning models into 3D-printable parts. *ACM Transactions on Graphics*, 2012, 31(6): 129:1-129:10.
- [10] Wang W, Wang T Y, Yang Z, Liu L, Tong X, Tong W, Deng J, Chen F, Liu X. Cost-effective printing of 3D objects with skin-frame structures. *ACM Transactions on Graphics*, 2013, 32(6): 177:1-177:10.
- [11] Lu L, Sharf A, Zhao H, Wei Y, Fan Q, Chen X, Savoye Y, Tu C, Cohen-Or D, Chen B. Build-to-last: Strength to weight 3D printed objects. *ACM Transactions on Graphics*, 2014, 33(4): 97:1-97:10.
- [12] Zhang X, Xia Y, Wang J, Yang Z, Tu C, Wang W. Medial axis tree — An internal supporting structure for 3D printing. *Computer Aided Geometric Design*, 2015, 35(c): 149-162.
- [13] Telea A, Jalba A. Voxel-based assessment of printability of 3D shapes. In *Proc. the 10th International Conference on Mathematical Morphology and Its Applications to Image and Signal Processing*, July 2011, pp.393-404.
- [14] Hašan M, Fuchs M, Matusik W, Pfister H, Rusinkiewicz S. Physical reproduction of materials with specified sub-surface scattering. *ACM Transactions on Graphics*, 2010, 29(4): 61:1-61:10.
- [15] Dong Y, Wang J, Pellacini F, Tong X, Guo B. Fabricating spatially-varying subsurface scattering. *ACM Transactions on Graphics*, 2010, 29(4): 153:1-153:10.
- [16] Papas M, Regg C, Jarosz W, Bickel B, Jackson P, Matusik W, Marschner S, Gross M. Fabricating translucent materials using continuous pigment mixtures. *ACM Transactions on Graphics*, 2013, 32(4): 146:1-146:12.
- [17] Chen D, Levin D I, Didyk P, Sitthi-Amorn P, Matusik W. Spec2Fab: A reducer-tuner model for translating specifications to 3D prints. *ACM Transactions on Graphics*, 2013, 32(4): 135:1-135:10.
- [18] Weyrich T, Peers P, Matusik W, Rusinkiewicz S. Fabricating microgeometry for custom surface reflectance. *ACM Transactions on Graphics*, 2009, 28(3): 32:1-32:6.
- [19] Levin A, Glasner D, Xiong Y, Durand F, Freeman W, Matusik W, Zickler T. Fabricating BRDFs at high spatial resolution using wave optics. *ACM Transactions on Graphics*, 2013, 32(4): 144:1-144:13.
- [20] Matusik W, Ajdin B, Gu J, Lawrence J, Lensch H, Pellacini F, Rusinkiewicz S. Printing spatially-varying reflectance. *ACM Transactions on Graphics*, 2009, 28(5): 128:1-128:10.
- [21] Dong Y, Tong X, Pellacini F, Guo B. Printing spatially-varying reflectance for reproducing HDR images. *ACM Transactions on Graphics*, 2012, 31(4): 40:1-40:8.
- [22] Malzbender T, Samadani R, Scher S, Crume A, Dunn D, Davis J. Printing reflectance functions. *ACM Transactions on Graphics*, 2012, 31(3): 20:1-20:11.
- [23] Lan Y, Dong Y, Pellacini F, Tong X. Bi-scale appearance fabrication. *ACM Transactions on Graphics*, 2013, 32(4): 145:1-145:12.
- [24] Vidimče K, Wang S P, Ragan-Kelley J, Matusik W. Open-Fab: A programmable pipeline for multi-material fabrication. *ACM Transactions on Graphics*, 2013, 32(4): 136:1-136:11.
- [25] Song P, Fu C, Cohen-Or D. Recursive interlocking puzzles. *ACM Transactions on Graphics*, 2012, 31(6): 128:1-128:10.
- [26] Xin S, Lai C, Fu C, Wong T, He Y, Cohen-Or D. Making burr puzzles from 3D models. *ACM Transactions on Graphics*, 2011, 30(4): 97:1-97:8.
- [27] Coros S, Thomaszewski B, Noris G, Sueda S, Forberg M, Sumner R W, Matusik W, Bickel B. Computational design of mechanical characters. *ACM Transactions on Graphics*, 2013, 32(4): 83:1-83:12.
- [28] Zhu L, Xu W, Snyder J, Liu Y, Wang G, Guo B. Motion-guided mechanical toy modeling. *ACM Transactions on Graphics*, 2012, 31(6): 127:1-127:10.

- [29] Ceylan D, Li W, Mitra N J, Agrawala M, Pauly M. Designing and fabricating mechanical automata from mocap sequences. *ACM Transactions on Graphics*, 2013, 32(6): 186:1-186:11.
- [30] Bäcker M, Bickel B, James D L, Pfister H. Fabricating articulated characters from skinned meshes. *ACM Transactions on Graphics*, 2012, 31(4): 47:1-47:9.
- [31] Cali J, Calian D A, Amati C, Kleinberger R, Steed A, Kautz J, Weyrich T. 3D-printing of non-assembly, articulated models. *ACM Transactions on Graphics*, 2012, 31(6): 130:1-130:8.
- [32] Chen Y, Chen Z. Joint analysis in rapid fabrication of non-assembly mechanisms. *Rapid Prototyping Journal*, 2011, 17(6): 408-417.
- [33] Su X, Yang Y, Wang D, Chen Y. Digital assembly and direct fabrication of mechanism based on selective laser melting. *Rapid Prototyping Journal*, 2013, 19(3): 166-172.
- [34] Cornea N D, Silver D, Min P. Curve-skeleton properties, applications, and algorithms. *IEEE Transactions on Visualization and Computer Graphics*, 2007, 13(3): 530-548.
- [35] Au O K C, Tai C L, Chu H K, Cohen-Or D, Lee T Y. Skeleton extraction by mesh contraction. *ACM Transactions on Graphics*, 2008, 27(3): 44:1-44:10.
- [36] Chuang M, Kazhdan M. Fast mean-curvature flow via finite-elements tracking. *Computer Graphics Forum*, 2011, 30(6): 1750-1760.
- [37] Tagliasacchi A, Alhashim I, Olson M, Zhang H. Mean curvature skeletons. *Computer Graphics Forum*, 2012, 31(5): 1735-1744.
- [38] Jiang W, Xu K, Cheng Z Q, Martin R R, Dang G. Curve skeleton extraction by coupled graph contraction and surface clustering. *Graphical Models*, 2013, 75(3): 137-148.
- [39] Dey T K, Sun J. Defining and computing curve-skeletons with medial geodesic function. In *Proc. the 4th Symposium on Geometry Processing*, June 2006, pp.143-152.
- [40] Hilaga M, Shinagawa Y, Kohmura T, Kunii T L. Topology matching for fully automatic similarity estimation of 3D shapes. In *Proc. the 28th Annual Conference on Computer Graphics and Interactive Techniques*, Aug. 2001, pp.203-212.
- [41] Katz S, Tal A. Hierarchical mesh decomposition using fuzzy clustering and cuts. *ACM Transactions on Graphics*, 2003, 22(3): 954-961.
- [42] Sharf A, Lewiner T, Shamir A, Kobbelt L. On-the-fly curve-skeleton computation for 3D shapes. *Computer Graphics Forum*, 2007, 26(3): 323-328.
- [43] Li G, Liu L, Zheng H, Mitra N J. Analysis, reconstruction and manipulation using arterial snakes. *ACM Transactions on Graphics*, 2010, 29(6): 152:1-152:10.
- [44] Cao J, Tagliasacchi A, Olson M, Zhang H, Su Z. Point cloud skeletons via Laplacian based contraction. In *Proc. International Conference on Shape Modeling and Applications*, June 2010, pp.187-197.
- [45] Livny Y, Yan F, Olson M, Chen B, Zhang H, El-Sana J. Automatic reconstruction of tree skeletal structures from point clouds. *ACM Transactions on Graphics*, 2010, 29(6): 151:1-151:8.
- [46] Tagliasacchi A, Zhang H, Cohen-Or D. Curve skeleton extraction from incomplete point cloud. *ACM Transactions on Graphics*, 2009, 28(3): 71:1-71:9.
- [47] Bucksch A, Lindenberg R, Menenti M. SkelTre. *The Visual Computer: International Journal of Computer Graphics*, 2010, 26(10): 1283-1300.
- [48] Natali M, Biasotti S, Patanè G, Falcidieno B. Graph-based representations of point clouds. *Graphical Models*, 2011, 73(5): 151-164.
- [49] Baran I, Popović J. Automatic rigging and animation of 3D characters. *ACM Transactions on Graphics*, 2007, 26(3): 72:1-72:8.
- [50] Beer F P, Jr. Russell Johnston E, DeWolf J T, Mazurek D F. *Mechanics of Materials (6th edition)*. New York: McGraw-Hill, 2012.



Wen-Peng Xu is a Ph.D. candidate at the School of Mathematical Sciences, University of Science and Technology of China, Hefei. He is also an associate professor in Henan Polytechnic University, Jiaozuo. His main research interests include computer graphics and 3D printing. He received his B.S. degree in mechanical engineering from Zhejiang University, Hangzhou, in 2004.



printing.

Wei Li received his B.S. degree in statistics from Northwestern Polytechnical University, Xi'an, in 2015. He is currently a master student of the School of Mathematical Sciences, University of Science and Technology of China, Hefei. His research interests include geometry processing, computer graphics and 3D



Li-Gang Liu is a professor at the School of Mathematical Sciences, University of Science and Technology of China, Hefei. He received his B.S. (1996) and Ph.D. (2001) degrees in applied mathematics from Zhejiang University, Hangzhou. Between 2001 and 2004, he worked at Microsoft Research Asia, Beijing. Then he worked at Zhejiang University during 2004 and 2012. He paid an academic visit to Harvard University during 2009 and 2011. He is on the editorial boards of *Computer Aided Geometric Design* and *IEEE Computer Graphics and Applications*, and was PC co-chair of *ACM Symposium on Solid and Physical Modeling 2014* and *Eurographics Symposium on Geometry Processing 2015*. His research interests include computer graphics and image processing.